ADVANCED OPTICAL MATERIALS
www.advopticalmat.de

Gold Nanohelices for Chiral Plasmonic Films by Templated Electroless Plating

*Po-Ting Chiu, Chih-Ying Yang, Zhi-Hong Xie, Ming-Yao Chang, Yu-Chueh Hung, and Rong-Ming Ho**

Chiral plasmonic films with gold nanohelices in polymer matrix are fabricated by templated electroless plating using self-assembled enantiomeric polylactide-based block copolymers (BCPs) as templates. By taking advantage of the helicity control of forming helical phase from the self-assembly of chiral BCPs, mirror-image signals from Cotton effect in electronic circular dichroism spectra can be clearly identified. The polymeric films with gold nanohelices show chiral plasmonic properties, as further evidenced by simulation from finite-difference time-domain method. This study may shed the light on fabrication of chiral plasmonic materials with adaptability in the applications for optical devices.

1. Introduction

The collective oscillation of free electrons in gold or silver nanoparticles is known as localized surface plasmon resonance (LSPR), whose origin has been extensively studied.[1] Recently, chiral metamaterials with chiral LSPR have drawn great attention for their applications in chirality detection,[2] beam splitters,[3] nanosensors,[2a,4] and biomedical treatments.[5] The asymmetric objects, patterns, and arrangements can absorb, scatter, or reflect right-handed circular polarization (RCP) or left-handed circular polarization (LCP) with respect to the inherent chirality of right- and left-handed textures, giving chiroptical responses with mirror image. Among all the chiral geometries, helix attracts most attention due to its obvious chiral sense with clockwise or counterclockwise rotation along helical axis. The geometry of helix is pitch length (*P*), helical diameter (*d*), and wire diameter (*t*), determining the corresponding chiral optics.[6] The top-down approach is widely used to acquire helical plasmonic metamaterials. Gansel et al. have fabricated a gold helix array by using the template from direct laser writing in micrometer scale as a broad band beam splitter in the range of 3 to 6 μm.[3a]

For the most desired regions of visible and near-infrared wavelengths due to the appealing potential for applications, Esposito et al. utilized bottom-up technologies to fabricate nanohelices on nanometer scale.[7] Focused ion or electron beam induced deposition can deposit metal–organic precursors on the sample surface to shape in designed helical structure with diameters of approximately 100 nm, resulting in the transmittance difference of LCP and RCP in the micrometer range for responsive wavelengths. To give a facile method for the fabrication of helical nano-objects, Mark et al. demonstrated the fabrication of chiral Au nanospirals by glancing angle deposition but with less ordered textures.[8] Huge electronic circular dichroism (ECD) responses can be observed with the responsive wavelengths in the range of sub-micrometer to several micrometers. Jeong et al. demonstrated the fabrication of plasmonic extinction and corresponding chiral optics of helical spirals with wire diameter of approximately 40 nm.[4] Huang et al. even fabricated Ag nanospirals which show interesting chiral responses.[8c,9] However, the oscillation modes of free electrons from the helical Au spirals fabricated and the corresponding chiroptic behaviors are still in debate. Also, it is noted that ECD contains both contributions from linear dichroism (LD) and ellipticity while most of the studies focus on the examination of LCP and RCP transmittance; thus, it could be difficult to justify how the free electrons in chiral Au nanostructures interact with the incident beam. To truly resolve the interactions of chiral LSPR from Au nanohelices, it is essential to acquire the spectra of the ECD and *g* factor with respect to the absorption of responsive wavelengths under negligible LD and linear birefringence (LB) effects.[10]

Block copolymers (BCPs) can serve as templates for templated electroless plating to fabricate Au nano-objects.[11] By tuning the molecular weight, the size of self-assembled texture can be tuned to give the templates with controlled dimension for the desired optical responses. Moreover, BCPs are well known for the processability of film fabrication, which is promising for the fabrication of optical devices. A unique helical phase (H*) with controlled helicity has been discovered in the self-assembly of polystyrene-*b*-poly(L-lactide) (PS-PLLA) chiral BCPs (denoted as BCPs*),[11a,12] which can be hydrolyzed for templated synthesis of a wide variety of nanostructured materials.[11a,13]

P.-T. Chiu, Prof. R.-M. Ho
Department of Chemical Engineering
National Tsing Hua University
No. 101, Section 2, Kuang-Fu Road, Hsinchu
Taiwan 300044, Republic of China
E-mail: rmho@mx.nthu.edu.tw
C.-Y. Yang, Z.-H. Xie, M.-Y. Chang, Y.-C. Hung
Institute of Photonics Technologies
National Tsing Hua University
No. 101, Section 2, Kuang-Fu Road, Hsinchu
Taiwan 300044, Republic of China
The ORCID identification number(s) for the author(s) of this article can be found under https://doi.org/10.1002/adom.202002133.

DOI: 10.1002/adom.202002133

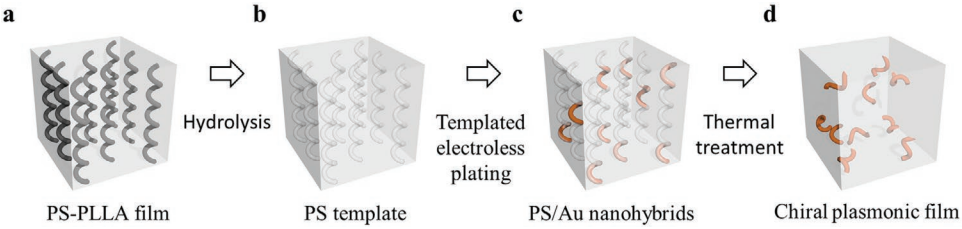

Figure 1. Schematic illustration of fabricating chiral plasmonic films with gold nanohelices in polymer matrix (PS/Au nanohybrids). a) PS-PLLA film after drop casting followed by solvent annealing; b) PS template with helical nanochannels after removal of PLLA block in the PS-PLLA by hydrolysis; c) Au nanohelices fabricated from templated electroless plating; d) PS/Au nanohybrids film after thermal treatment to melt away unfilled pores.

Herein, we aim to use hydrolyzed H* from polylactide-based BCPs* with helical nanochannels as templates for templated electroless plating. Isolated Au nanohelices dispersed in the PS matrix can be fabricated for chiroptic films with responsive wavelength in the visible region. Solutions of PS-PLLA and polystyrene-*b*-poly(D-lactide) (PS-PDLA) are drop cast into films on silicon wafer followed by solvent annealing to give self-assembled helical phase (**Figure 1**a). Polylactide block in the BCPs* is further hydrolyzed in basic solution to create a template with helical nanochannels (Figure 1b). Templated electroless plating will be carried out to fabricate Au nanohelices with specific handedness (Figure 1c). The unfilled voids are then demolished by heating the samples over the glass transition temperature of the PS to alleviate light scattering problem from nanoporous texture, giving the authentic optical responses from the fabricated Au nanohelices in polystyrene matrix (Figure 1d).

2. Results and Discussion

PS-PLLA (Mn = 20 300 g mol^{-1}, Đ = 1.12, f_{PLLA}^{v} = 0.37) and PS-PDLA (Mn = 21 100 g mol^{-1}, Đ = 1.13, f_{PLLA}^{v}= 0.39) samples with equivalent molecular weight were synthesized (see Supporting Information for details), and used as templates after hydrolysis for templated electroless plating. As shown in **Figure 2**a,b, transmission electron microscopy (TEM) projections of RuO_4-stained samples with the bright polylactide helical structures hexagonally packed in the dark PS matrix as further confirmed by 1D small-angle X-ray scattering (SAXS) (Figure 2c,d) where the characteristic reflections at the relative q values of $1:\sqrt{4}:\sqrt{7}$ can be clearly identified. To fabricate plasmonic films, the synthesized samples were cast into films with thickness of approximately 50 µm followed by solvent annealing for self-assembly. To acquire higher degree of structural order, solvent annealing was conducted in a jar for ten days under ambient condition followed by a slow evaporation rate to remove the residual solvent. Subsequently, the BCP films were immersed in a mixture of aqueous sodium hydroxide and methanol to hydrolyze polylactide in the BCP for the fabrication of templates with nanoporous helical texture. **Figure 3**a,b shows the SEM top views of the templates fabricated at which the nanochannels can be clearly recognized with crescent-like texture and hexagonally packed pores from hydrolyzed helices.

After templated electroless plating, the Au nanohelices replicate the size and the shape of the nanoporous texture of the templates. For templated electroless plating of reduced metal ions, the formation of the reduced Au was carried out through nucleation and growth due to the highest reduction potential of Au ion, giving self-nucleation followed by growth for the formation of Au nanoobject from templating. Moreover, it is necessary to consider the forming texture with a homogeneous distribution in the PS template to give reliable and reproducible chiroptical responses. It is noted that the diffusion of Au ions from the solution to the center part of the template is much more difficult in tubular helical nanochannels than that in the nanochannels with continuity such as network-structured ones due to the difficulties of driving the air out of the nanochannels. Film fabricated from solvent annealing might fulfill the criteria to give open-cell character after solvent evaporation for aimed templated electroless plating at which the interruption of blocking can be minimized and the fabricated films can be much more applicable for chiroptic devices although it might cause the variation of pitch length. Figure 3c,d shows the TEM

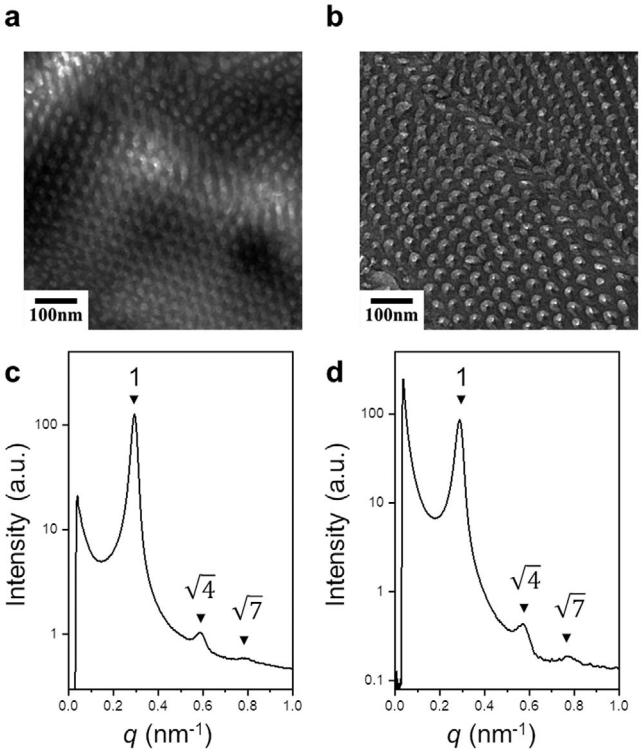

Figure 2. TEM images and SAXS profiles of PS-PLLA and PS-PDLA. Typical TEM projections of helical phases from a) PS-PLLA and b) PS-PDLA. c,d) Corresponding SAXS profiles with characteristic reflections of hexagonally packed helices of (a) and (b), respectively.

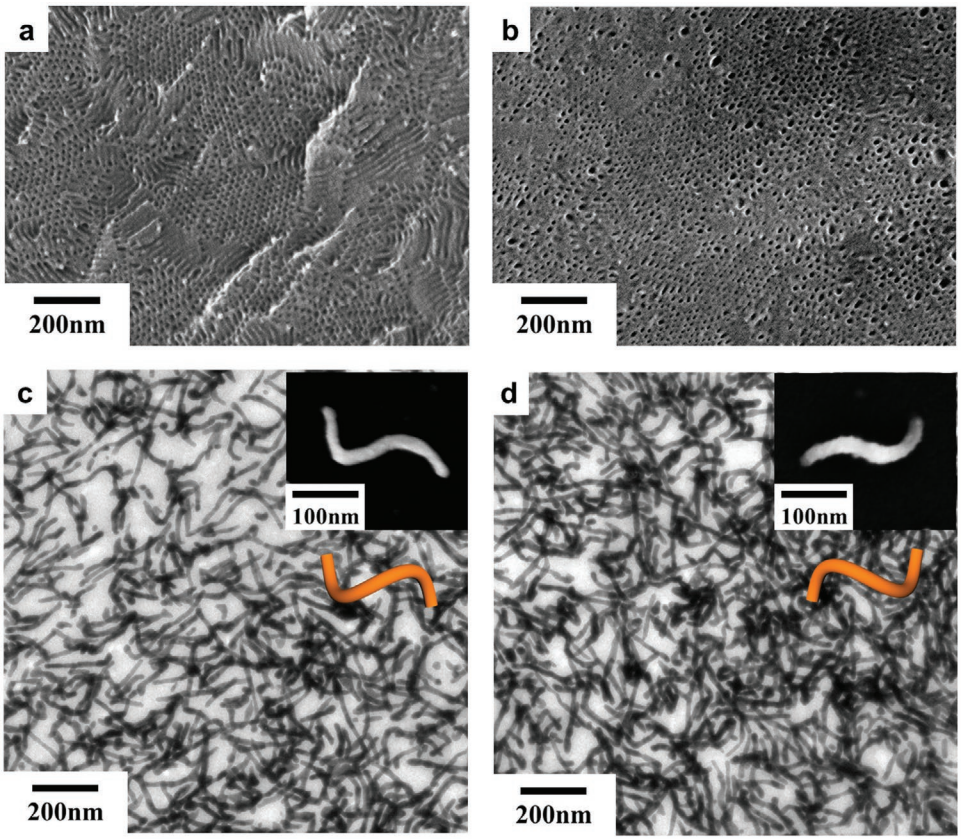

Figure 3. SEM micrographs of top-view templates from self-assembled a) PS-PLLA and b) PS-PDLA after hydrolysis. c,d) TEM micrographs of Au nanohelices fabricated from (a) and (b), respectively. Insets are the corresponding isolated Au nanohelices from templated electroless plating after removal of the templates: c) left-handed Au nanohelices fabricated from PS-PLLA and d) right-handed Au fabricated from PS-PDLA.

images of left- and right-handed Au nanohelices fabricated by using templates of Figure 3a,b, respectively. To visualize the fabricated Au nanohelices and to examine the corresponding handedness, removal of PS template was carried out by exposing the films to UV/O_3 for three days followed by O_2 reactive-ion etching (RIE). The curve of helical contour can be clearly observed by SEM (insets in Figure 3c,d) and TEM (Figure S1, Supporting Information) from the individual Au nanohelices. Notably, the sizes of the helices are not the same as the sizes in the templates. In fact, as the PS template was removed, the Au nanohelices might straighten and thicken. Before complete removal of the PS matrix, the helix retained its texture with P of approximately 100 nm, d of approximately 70 nm, and t of approximately 28 nm (Figure S2a, Supporting Information). Yet, the helical shape might start to relax after releasing from the PS for three days, and the size would change accordingly, giving barely recognizable helicity with larger dimension at which the wire diameter can even reach 50 nm (Figure S2b, Supporting Information). As the relaxation time extended to seven days, the Au nanohelices no longer exist; only a nanorod with d of approximately 50 nm can be observed (Figure S2c, Supporting Information). The tendency of transforming from helix to thicker cylindrical rod after removal of the PS template might be attributed to the rearrangement of Au atoms after exposure to UV/O_3 and O_2 RIE during removal of the PS template, which could temporally oxidize the Au atoms and give the atoms enough energy for its mobility.[14] Accordingly, the defects might be generated, and the minimization of surface defects could occur to give higher thermodynamic stability of the individual nanoobject by changing the shape from helix to cylinder. As a result, the PS matrix might be essential to retain the textures of Au nanohelices and to provide the dielectric matrix for expected chiral responses.

To acquire the signals of ECD purely originating from the randomly distributed Au nanohelices in the solid-film state, the hybrid bulk film was heated to 120 °C for melting away the unfilled nanochannels. **Figure 4**a shows the ECD and UV–Vis spectra of the plasmonic films with Au helices in a PS matrix on quartz substrates. Although the density of Au nanohelices is high, the coupling effect between each Au nanohelix should be trivial for the inter distance of helical channels of approximately 20 nm based on SAXS results. The UV–Vis spectra from left- and right-handed samples show similar profiles. There are two observable absorption bands at 550 and 610 nm which can be assigned as the LSPR of Au nanohelices. Based on the electric field distributions of these two bands, the dipole distributions at 550 nm exhibit the transverse mode character while the dipoles at 610 nm show the longitudinal mode.[15] Dipole–dipole interaction may give rise to the difference of circular dichroism behaviors of the two bands. Since the BCPs* used in this study have similar molecular weights, the dimension of Au nanohelices fabricated should be equivalent, resulting in similar absorption

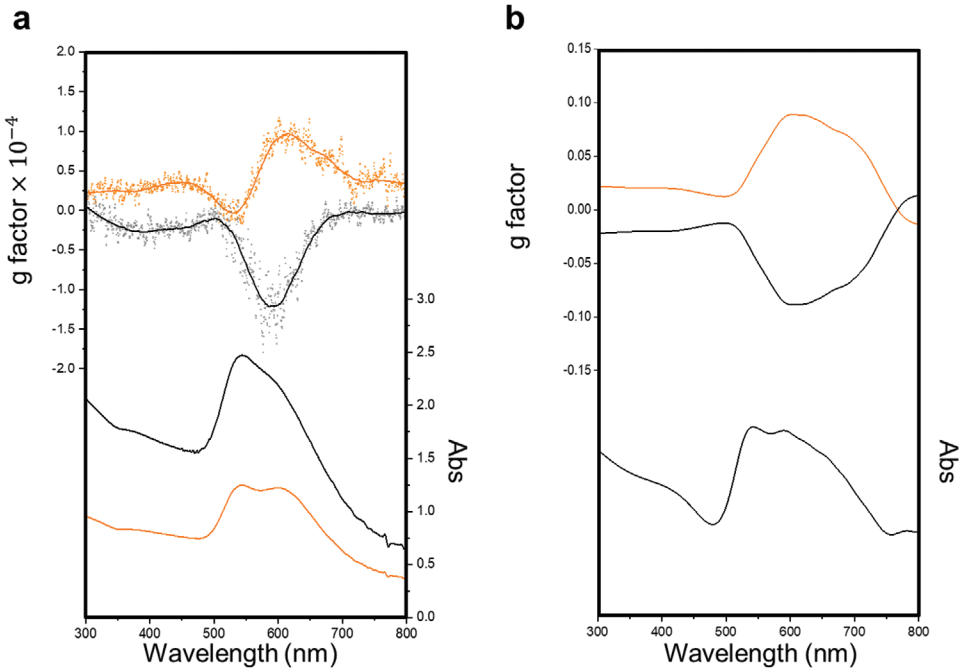

Figure 4. Experimental and simulated ECD and UV–Vis spectra of left- and right-handed Au nanohelices in PS matrix. a) Experimental solid-state ECD spectra of left-handed Au (orange) and right-handed Au (black) in PS matrix and the corresponding UV–Vis spectra. b) Simulated ECD and UV–Vis spectra using the sizes measured from SEM results.

bands. To minimize the thickness effect on ECD signal, the signals were converted into *g* factor. Mirror image of ECD signals can be clearly observed in Figure 4a, in which the orange and the black ones are contributed by left- and right-handed Au nanohelices, respectively. The transverse resonance mode contributes no significant signal, whereas the most significant ECD signals approximately match the longitudinal mode at 610 nm. The ECD signals observed in this study are assigned as Cotton effect instead of a split-type Cotton effect for the direct connection between the signals and the absorption bands at 610 nm.[10b] Figure S3, Supporting Information, shows the corresponding LD spectra from 300 to 800 nm well below 0.005, indicating that there should be no observable anisotropic effect on spectroscopic measurements in the films. Besides LD, another factor that may affect the circular dichroism (CD) measurements is LB. To exclude this effect, observation under polarized light microscopy (PLM) with gypsum plate is required. As shown in Figure S4a,b, Supporting Information, the color from left-handed Au was dark blue at 0° whereas the same color was observed at 90°. Similar results were acquired from right-handed Au (Figure S4c,d, Supporting Information). Meanwhile, the bright (Figure S4e,g, Supporting Information) and dark (Figure S4,h, Supporting Information) images under PLM with two polarizers were observed at parallel and crossed position, respectively. These results indicate that the LB effect is null.

Figure 4b shows the simulations for ECD and absorption spectra from Au nanohelices in PS matrix by finite-difference time-domain (FDTD) method. Since the size of helix is not a constant in BCP* where the *p* and *d* might vary from domain to domain due to the sample preparation and electroless plating, the dimensions of helix used for simulation are some representative values obtained from SEM images. The simulated results contain absorption and scattering of Au nanohelices (the separate contribution of absorption and scattering, and the corresponding CD spectra are shown in Figure S5, Supporting Information) which are similar to the experimental condition. The ECD signals range from 600 to 700 nm, which are in line with the measured results. The intersection of simulated ECD signals beyond 700 nm are not observed experimentally; the reason might be the scattering of the film which makes those small signals not observable. The absorption spectrum shows one peak at 550 nm, which corresponds to the LSPR of Au. Another broadband ranges from 600 to 730 nm, which matches the wavelengths of the experimental CD signals. Notably, there is a small ratio of Au nanohelices with long pitch length as found experimentally which contributes no CD signal but only the absorption near 630 nm. Based on the wide CD signals and the absorption band in simulation and experimental results, we speculate that the dimensions of helix are indeed not constant. Compared to other helical systems (*g* factor of approximately 0.001),[16] the *g* factor of 0.0001 in this study is low. The reason might be the scattering from the heterogeneous film with reduced gold in the PS matrix which leads to significant background in absorption spectra, resulting in the reduction in the value of *g* factor. Another possible reason is the incomplete preservation of helical character after melting away the residual voids that might cause the relaxation of Au nanohelices. We speculate that those drawbacks might be alleviated by reducing the thickness of the thin-film hybrids with uniform surface and controlling the orientation of the helical phase for templated electroless plating. In the simulation, where perfect helical geometries were used, the value of simulated *g* factor is quite large compared to the experimental one. The potential of Au nanohelices for application is promising when the helical textures could be well-duplicated.

3. Conclusion

In conclusion, plasmonic polymeric films with chiral Au nanohelices imbedded were fabricated through templated electroless plating using self-assembled PS-PLLA/PS-PDLA as templates. The chirality of nanohelices can be controlled by the choice of chiral PLLA/PDLA block. The films exhibit plasmonic effects from Au nanohelices with controlled chiroptical response: positive and negative ECD signals in visible wavelengths from left- and right-handed Au nanohelices, respectively, which is further confirmed by FDTD simulation. This study provides a new strategy of fabricating chiral plasmonic materials from a polymer-based bottom-up approach. By taking advantage of the processability of polymer film, a scalable method for the fabrication of chiral metamaterials in the applications such as bio-sensing can be established.

4. Experimental Section

Synthesis of Templates: PS–PLLA diblock copolymers were synthesized by a double-headed initiator through two-step polymerization: atom transfer radical and ring-opening polymerization in sequence.[17] Different enantiomeric isomers of lactides, including L-lactide (purity > 98.0%) and D-lactide (purity > 98.0%), were purchased from TCI and Combi-Blocks, respectively. Stannous 2-ethylhexanoate, purchased from Aldrich, was diluted in toluene before use. For the synthesis of PS–PLLA and PS–PDLA, 0.1 g PS with hydroxyl chain end, 0.09 g lactide, 8 mg $Sn(Oct)_2$ and 1 mL dry toluene were added in a dry glass flask equipped with a magnetic stirrer, and heated to 115 °C for 3 h. The reaction was quenched by methanol at 0 °C. After drying under vacuum, PS–PLLA and PS–PDLA powder was obtained. Bulk films of PS–PLLA and PS–PDLA samples were drop cast on wafers from CH_2Cl_2 solution, followed by solvent annealing using CH_2Cl_2 for ten days, and then quenched to ambient environment. Hydrolysis was then carried out to degenerate the PLLA or PDLA domain for the formation of helical nanochannels.

Electroless Plating: Au nanohelices were synthesized by templated electroless plating as described in the previous study.[11c] At the nucleation stage, Au nanoparticles were reduced from Au ion (Au^{+3}) with the presence of reducing agent (hydrazinium hydroxide, N_2H_5OH), giving randomly seeded Au nanoparticles in the nanoporous PS template. The Au ion solution was prepared by dissolving 0.05 g hydrogen tetrachloroaurate(III) trihydrate into 20 mL methanol. The PS templates were left in the solution overnight and transferred to $N_2H_5OH(aq)$. In the templated growth process, weak reducing agent (diethanolamine, DEA) was then used to ensure that the reducing Au starts from the nuclei followed by growth for filling up the nanochannels to form nanohelices. The growing solution was prepared by mixing 0.05 g hydrogen tetrachloroaurate(III) trihydrate, 0.1 g DEA, and 0.1 mL HCl in 20 mL methanol. The PS templates with Au nuclei were left in the growing solution for two days to obtain the Au nanohelices.

Transmission Electron Microscopy: Bright-field TEM images were obtained with a JEOL JEM-2100 LaB_6 transmission electron microscope (at an accelerating voltage of 200 kV). Images were recorded on a Gatan CCD camera. The bulk samples of PS–PLLA, PS–PDLA, and PS/Au were sectioned at room temperature by Leica Ultra-microtome with the thickness of 100 nm. Afterward, the microsections were collected on copper grids (100 mesh). For PS-PLLA/PS-PDLA samples, PS was stained by RuO_4 to create the contrast from PLLA or PDLA. Staining was not necessary for PS/Au since electron density of Au was large enough as compared to PS to give significant mass-thickness contrast.

Measurements of ECD, LD, and UV-Vis Spectra: The bulk film samples were positioned on quartz for the measurements. Before acquiring the spectra, the samples were annealed at 140 °C to melt away the unfilled pores, giving homogeneous PS matrix. ECD, LD, and UV–Visible spectra were performed using a JASCO J-815 spectrometer at room temperature. Scanning parameters were set as: scanning speed, 100 nm min^{-1}; digital integration time, 4 s; three accumulation; data pitch, 0.1 nm; bandwidth, 1 nm. The anisotropy g factor was calculated according to the following equation: $g = \frac{CD}{32980 \times abs}$, where abs is the absorption.

Simulation of Absorption and Corresponding CD Spectrum: The simulation of the absorption UV and corresponding CD spectrum was performed by a 3D electromagnetic solver (FDTD Solutions, Lumerical Inc.).[18] To simulate optical responses of a single helix, the boundary conditions were set to be perfectly matched layer. Two total-field scattered-field sources with polarization angle and phase difference were used to generate circularly polarized light. Two analysis groups using frequency-domain profile and power monitors were employed to calculate the absorption and scattering. A uniform mesh size of 5-nm was employed after the convergence test for Au helix simulations. The refractive index of PS was 1.6. The refractive index of Au was from the study of Johnson and Christy.[19] The circularly polarized light was incident from *x*-axis and the helix structures were rotated along *y*-axis and *z*-axis. Spectra were recorded for helices rotated every 15° from 0° to 45° for *y*-axis and 45° to 90° for *z*-axis, where the CD and absorption spectra were averaged over 16 orientations.

Supporting Information

Supporting Information is available from the Wiley Online Library or from the author.

Acknowledgements

The authors would like to thank the Ministry of Science and Technology (MOST), Taiwan, for financially supporting this research under Contract No. MOST 107-2221-E-007-030-MY3 and MOST 107-2923-M-007-003-MY3. The authors would like to thank the National Synchrotron Radiation Research Center (NSRRC) for its assistance in the synchrotron SAXS experiments. The authors would like to thank Instrumentation Center at NTHU for NMR experiments.

Conflict of Interest

The authors declare no conflict of interest.

Data Availability Statement

The data that support the findings of this study are openly available in figshare at http://doi.org/10.6084/m9.figshare.14189027, reference number 1–4.

Keywords

block copolymers, chirality, electroless plating, localized surface plasmon resonance, nanohelix

Received: December 13, 2020
Revised: February 25, 2021
Published online: March 24, 2021

[1] a) S. Link, M. A. El-Sayed, *J. Phys. Chem. B* **1999**, *103*, 4212; b) S. Eustis, M. A. El-Sayed, *Chem. Soc. Rev.* **2006**, *35*, 209.
[2] a) X. Kuang, S. Ye, X. Li, Y. Ma, C. Zhang, B. Tang, *Chem. Commun.* **2016**, *52*, 5432; b) Y. Zhao, A. N. Askarpour, L. Sun, J. Shi, X. Li, A. Alù, *Nat. Commun.* **2017**, *8*, 14180; c) X. Wu, C. Hao, J. Kumar,

H. Kuang, N. A. Kotov, L. M. Liz-Marzán, C. Xu, *Chem. Soc. Rev.* **2018**, *47*, 4677.

[3] a) J. K. Gansel, M. Thiel, M. S. Rill, M. Decker, K. Bade, V. Saile, G. von Freymann, S. Linden, M. Wegener, *Science* **2009**, *325*, 1513; b) B. P. Cumming, G. E. Schröder-Turk, M. Gu, *Opt. Lett.* **2018**, *43*, 863.

[4] a) H.-H. Jeong, A. G. Mark, M. Alarcón-Correa, I. Kim, P. Oswald, T.-C. Lee, P. Fischer, *Nat. Commun.* **2016**, *7*, 11331; b) H.-H. Jeong, A. G. Mark, P. Fischer, *Chem. Commun.* **2016**, *52*, 12179.

[5] X. Huang, P. K. Jain, I. H. El-Sayed, M. A. El-Sayed, *Plasmonics* **2007**, *2*, 107.

[6] a) Y. Li, R. Ho, Y. Hung, *IEEE Photonics J.* **2013**, *5*, 2700510; b) A. Passaseo, M. Esposito, M. Cuscunà, V. Tasco, *Adv. Opt. Mater.* **2017**, *5*, 1601079.

[7] a) M. Esposito, V. Tasco, F. Todisco, A. Benedetti, D. Sanvitto, A. Passaseo, *Adv. Opt. Mater.* **2014**, *2*, 154; b) M. Esposito, V. Tasco, F. Todisco, M. Cuscunà, A. Benedetti, D. Sanvitto, A. Passaseo, *Nat. Commun.* **2015**, *6*, 6484; c) M. Esposito, V. Tasco, F. Todisco, M. Cuscunà, A. Benedetti, M. Scuderi, G. Nicotra, A. Passaseo, *Nano Lett.* **2016**, *16*, 5823.

[8] a) A. G. Mark, J. G. Gibbs, T.-C. Lee, P. Fischer, *Nat. Mater.* **2013**, *12*, 802; b) F. Bai, J. Deng, M. Yang, J. Fu, J. Ng, Z. Huang, *Nanotechnology* **2016**, *27*, 115703; c) J. Liu, L. Yang, Z. Huang, *Small* **2016**, *12*, 5902.

[9] J. Deng, J. Fu, J. Ng, Z. Huang, *Nanoscale* **2016**, *8*, 4504.

[10] a) S. C. Bjorling, R. A. Goldbeck, S. J. Milder, C. E. Randall, J. W. Lewis, D. S. Kliger, *J. Phys. Chem.* **1991**, *95*, 4685; b) N. Berova, K. Nakanishi, R. W. Woody, *Circular Dichroism: Principles and Applications*, John Wiley & Sons, New York **2000**.

[11] a) R.-M. Ho, Y.-W. Chiang, C.-K. Chen, H.-W. Wang, H. Hasegawa, S. Akasaka, E. L. Thomas, C. Burger, B. S. Hsiao, *J. Am. Chem. Soc.* **2009**, *131*, 18533; b) M.-S. She, T.-Y. Lo, H.-Y. Hsueh, R.-M. Ho, *NPG Asia Mater* **2013**, *5*, e42; c) H.-Y. Hsueh, H.-Y. Chen, Y.-C. Hung, Y.-C. Ling, S. Gwo, R.-M. Ho, *Adv. Mater.* **2013**, *25*, 1780; d) H.-Y. Hsueh, H.-Y. Chen, Y.-C. Ling, W.-S. Huang, Y.-C. Hung, S. Gwo, R.-M. Ho, *J. Mater. Chem. C* **2014**, *2*, 4667; e) H.-Y. Hsueh, C.-T. Yao, R.-M. Ho, *Chem. Soc. Rev.* **2015**, *44*, 1974.

[12] a) R.-M. Ho, M.-C. Li, S.-C. Lin, H.-F. Wang, Y.-D. Lee, H. Hasegawa, E. L. Thomas, *J. Am. Chem. Soc.* **2012**, *134*, 10974; b) T. Wen, H.-F. Wang, M.-C. Li, R.-M. Ho, *Acc. Chem. Res.* **2017**, *50*, 1011; c) H.-F. Wang, K.-C. Yang, W.-C. Hsu, J.-Y. Lee, J.-T. Hsu, G. M. Grason, E. L. Thomas, J.-C. Tsai, R.-M. Ho, *Proc. Natl. Acad. Sci. USA* **2019**, *116*, 4080.

[13] a) R.-M. Ho, Y.-W. Chiang, C.-C. Tsai, C.-C. Lin, B.-T. Ko, B.-H. Huang, *J. Am. Chem. Soc.* **2004**, *126*, 2704; b) W.-H. Tseng, C.-K. Chen, Y.-W. Chiang, R.-M. Ho, S. Akasaka, H. Hasegawa, *J. Am. Chem. Soc.* **2009**, *131*, 1356.

[14] G. Chandrasekar, K. Mougin, H. Haidara, L. Vidal, E. Gnecco, *Appl. Surf. Sci.* **2011**, *257*, 4175.

[15] a) C. L. Nehl, J. H. Hafner, *J. Mater. Chem.* **2008**, *18*, 2415; b) J. Ryu, S.-H. Lee, Y.-H. Lee, Y.-H. Chang, J.-W. Jang, *J. Phys. Chem. C* **2019**, *123*, 5626.

[16] J. Gao, W. Wu, V. Lemaire, A. Carvalho, S. Nlate, T. Buffeteau, R. Oda, Y. Battie, M. Pauly, E. Pouget, *ACS Nano* **2020**, *14*, 4111.

[17] K.-C. Yang, R.-M. Ho, *ACS Macro Lett.* **2020**, *9*, 1130.

[18] Lumerical Inc., https://www.lumerical.com/products/.

[19] P. B. Johnson, R. W. Christy, *Phys. Rev. B* **1972**, *6*, 4370.